Journal of Applied Physics

RESEARCH ARTICLE | MAY 06 2015

The conductivity mechanism and an improved C−V model of ferroelectric PZT thin film

K. Liang; A. Buditama; D. Chien; J. Cui; P. L. Cheung; S. Goljahi; S. H. Tolbert; J. P. Chang; C. S. Lynch

J. Appl. Phys. 117, 174107 (2015)
https://doi.org/10.1063/1.4919431

View Online

Export Citation

Articles You May Be Interested In

Switchable diode effect in ferroelectric thin film: High dependence on poling process and temperature

AIP Advances (December 2014)

Residual stress effects on piezoelectric response of sol-gel derived lead zirconate titanate thin films

J. Appl. Phys. (January 2007)

Photoelectron spectroscopic and microspectroscopic probes of ferroelectrics

AIP Conf. Proc. (December 2017)

20 January 2026 12:52:18

JOURNAL OF APPLIED PHYSICS 117, 174107 (2015)

The conductivity mechanism and an improved C–V model of ferroelectric PZT thin film

K. Liang,[1,2] A. Buditama,[3] D. Chien,[4] J. Cui,[1] P. L. Cheung,[4] S. Goljahi,[1] S. H. Tolbert,[3] J. P. Chang,[4] and C. S. Lynch[1,a)]

[1]*Department of Mechanical and Aerospace Engineering, University of California, Los Angeles, California 90095, USA*

[2]*Ministry of Education Key Laboratory for the Green Preparation and Application of Functional Materials, Hubei Collaborative Innovation Center for Advanced Organic Chemical Materials, School of Material Science and Engineering, Hubei University, Wuhan, 430062, China*

[3]*Department of Chemistry and Biochemistry, University of California, Los Angeles, California 90095, USA*

[4]*Department of Chemical and Biomolecular Engineering, University of California, Los Angeles, California 90095, USA*

(Received 27 January 2015; accepted 18 April 2015; published online 6 May 2015)

A dense, homogeneous and crack-free ferroelectric PZT thin film with ⟨100⟩-preferred orientation was produced using the sol-gel method. The volume fraction $\alpha_{(100)}$ of ⟨100⟩-oriented grains in the PZT film was calculated [$\alpha_{(100)} \approx 80\%$] from XRD of the PZT thin film and powder. The PZT thin film exhibits an open polarization vs. electric field loop and a low leakage current density from 10^{-8} A/cm^2 to 10^{-7} A/cm^2. The electrical conduction data were fit to a Schottky-emission model with deep traps from 100 kV/cm to 250 kV/cm. A modified capacitance model was introduced that adds electrical domain capacitance based on a metal-ferroelectric-metal (MFM) system with Schottky contacts. The model reproduces the observed non-linear capacitance vs. voltage behavior of the film. © *2015 AIP Publishing LLC*. [http://dx.doi.org/10.1063/1.4919431]

20 January 2026 12:52:18

I. INTRODUCTION

Thin film ferroelectrics with the perovskite structure have applications in nonvolatile memory, piezoelectric devices, electro-optics, and micro-mechanical systems.[1–4] The control of bistable and switchable polarization states in ferroelectrics underlies many of these applications. The fast and electrically switchable polarization of lead zirconate titanate [$Pb(Zr_{1-x}Ti_x)O_3$, PZT] has been extensively investigated.[5–8] Ferroelectric PZT thin films with compositions close to the morphotropic phase boundary (MPB) [$Pb(Zr_{0.52}Ti_{0.48})O_3$] exhibit enhanced properties.[9,10] The current vs. voltage (*I–V*) and capacitance vs. voltage (*C–V*) characteristics provide fundamental information about the polarization switching behavior and the conduction mechanism. Several models have been established to interpret the *I–V* and *C–V* characteristics.[11–13] However, the effect of electric field magnitude on the MFM structure has not received much attention, and the contribution of the effect of domain capacitance has not, to our knowledge, been included in a capacitive equivalent circuit model for ferroelectric thin films. In this work, a $Pb(Zr_{0.52}Ti_{0.48})O_3$ thin film was prepared using the sol-gel method and the *I–V* and *C–V* characteristics were measured. A capacitance model that includes the effect of MFM interfaces and domain capacitance was used to model the observed behavior.

II. EXPERIMENTAL

The chemical reagents used in this work were lead(II) acetate trihydrate [$Pb(CH_3COO)_2$–$3H_2O$], 2-methoxyethanol [$CH_3OCH_2CH_2OH$], zirconium(IV) propoxide [$Zr(CH_2CH_2CH_3)_4$], and titanium(IV) ethoxide [$Ti(CH_3CH_2O)_4$]. All chemicals were analytical grade purity of 99.99% and were used as received without further purification.

$Pb(Zr_{0.52}Ti_{0.48})O_3$ thin films were deposited on Pt(111)/Ti/SiO_2/Si(100) substrate using a sol-gel process. The precursor solution for the coating was prepared by a modified 2-methoxyethanol (2MOE) synthesis method:[14,15] dissolving appropriate amounts of $Pb(CH_3COO)_2{\cdot}3H_2O$ into 2MOE solution by magnetic stirring for 2 h, followed by stoichiometric addition of $Zr(CH_2CH_2CH_3)_4$ and $Ti(CH_3CH_2O)_4$ into the solution with further magnetic stirring over 12 h. 10 mol. % excess $Pb(CH_3COO)_2{\cdot}3H_2O$ was added to compensate the Pb loss during annealing. The PZT precursor solution was spin coated with a SCS G3 spin coater (Specialty Coating Systems INC.) on the Pt/Ti/SiO_2/Si substrates at 4000 rpm for 60 s, followed by pyrolysis at 300 °C for 1 min on a hot plate in air. After every four layers, a rapid thermal process was performed at 700 °C for 1 min in air. Solution coating and firing were repeated to produce PZT thin films with 12 layers. In addition, dried gel was prepared from the coating solution, and PZT powders were obtained by sintering the dried gel at 600 °C for 2 h in air. Au top electrodes were deposited by means of sputtering using a shadow mask with the size of 1 mm × 1 mm for each point to create parallel plate capacitors in PZT thin films. A typical thickness of the top electrodes was 200 nm. The crystal structures of the PZT film and powder were examined using X-ray diffraction (XRD, Bruker D8) with Cu K_α radiation ($\lambda = 1.54176$ Å) at the scanning rate of 5°/min from 20° to 55°. A Field-Emission Scanning Electron Microscope (FESEM, JSM-6700F) was used to observe the surface and cross-section of the PZT film. P–E and *I–V* measurements were

a)Author to whom correspondence should be addressed. Electronic mail: cslynch@seas.ucla.edu

 © 2015 AIP Publishing LLC

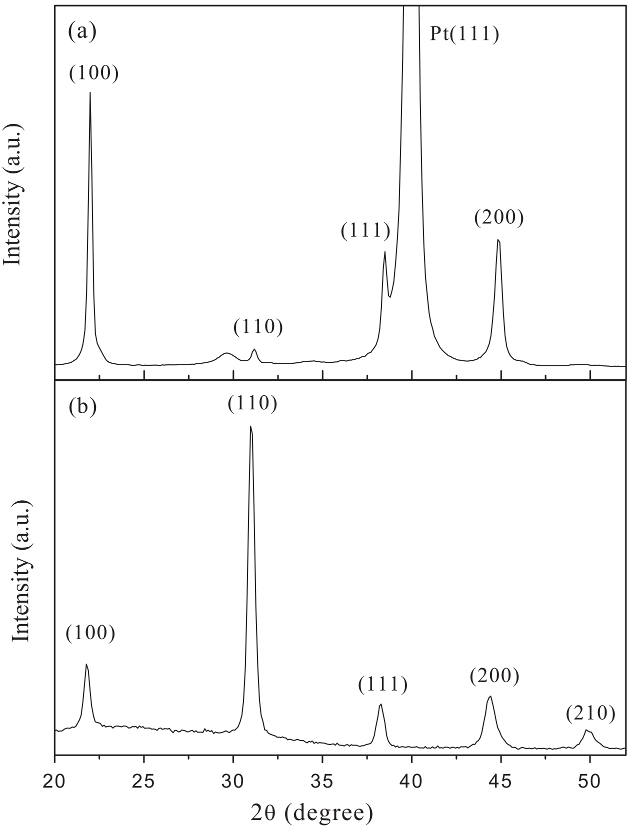

FIG. 1. XRD patterns of (a) PZT thin film and (b) PZT powder.

performed on the PZT capacitors using a ferroelectric test system (Radiant Technology Precision LC Materials Analyzer). A low-frequency impedance analyzer (HP-4284A) was employed to measure the *C–V* characteristics of the PZT capacitor.

III. RESULTS AND DISCUSSION

Figures 1(a) and 1(b) show the XRD patterns of the PZT thin film and powder. The {110} reflection is the strongest peak in Fig. 1(b) for the powder sample of random orientation. But the {100} reflections are much higher than the {110} peak in Fig. 1(a); the reflection {100} is the strongest peak. This indicates that the PZT film corresponding to Fig. 1(a) is of ⟨100⟩-preferred orientation. For a Zr/Ti ratio is 52/48, the growth planes with the lowest activation energy are {100}-planes.[16] This results in the formation of PZT thin film with ⟨100⟩-preferred orientation. In order to determine the degree of preferred orientation, the volume fraction $\alpha_{(h00)}$ of {h00} oriented grains in PZT film was approximated as[17]

$$\alpha_{(h00)} = \sum(I_{n00}/I^*_{n00})/\sum(I_{hkl}/I^*_{hkl}), \qquad (1)$$

where I_{hkl} is the measured intensity of the (*hkl*) peak for the film, I_{hkl}* is the intensity for powder, and n is the number of reflections. The α value for the PZT thin film is $\alpha_{(h00)} \approx 80\%$.

Figure 2 shows SEM micrographs of surface and cross-section of the PZT film. A dense, homogeneous, and crack-free PZT thin film is observed in Fig. 2(a), and the average width of grains in the columnar structure is approximately 30 nm. The thickness of the PZT film is about 750 nm based on the cross-sectional SEM image in Fig. 2(b). This value was used to determine the coercive field from the ferroelectric measurement. The polarization–field loop of the PZT thin film measured at room temperature with the frequency of 1 kHz is shown in Fig. 3. The $2P_r$ and $2E_c$ of the PZT thin film are 28 μC/cm^2 and 240 kV/cm, respectively, which are similar to the results reported by Bassiri-Gharb *et al.*[18] and Nguyen *et al.*[19]

Figure 4 illustrates the leakage current density as a function of electric field of the ferroelectric PZT thin film (*J–E* curve, based on the *I–V* behavior measured at a DC bias from 0 to 20 V). The initial linear part of the *J-E* curve appears ohmic up to about 100 kV/cm. A linear ln$J$–$E^{1/2}$ plot is obtained (see the inset of Fig. 4), which is characteristic of the Schottky-emission model with deep traps. In the Schottky-emission model, the current is given by[20]

$$J = A^{**}T^2 \exp\left[\frac{-q\left(\phi_B - \sqrt{qE/4\pi\varepsilon_0\varepsilon_r}\right)}{K_B T}\right], \qquad (2)$$

20 January 2026 12:52:18

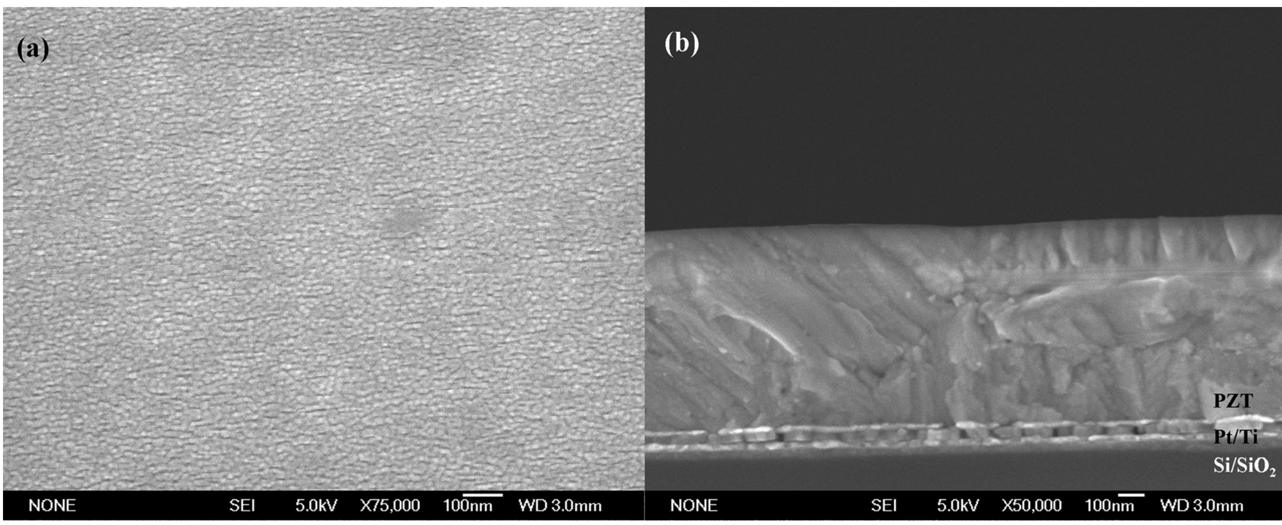

FIG. 2. (a) Surface and (b) cross-section of SEM images of PZT thin film.

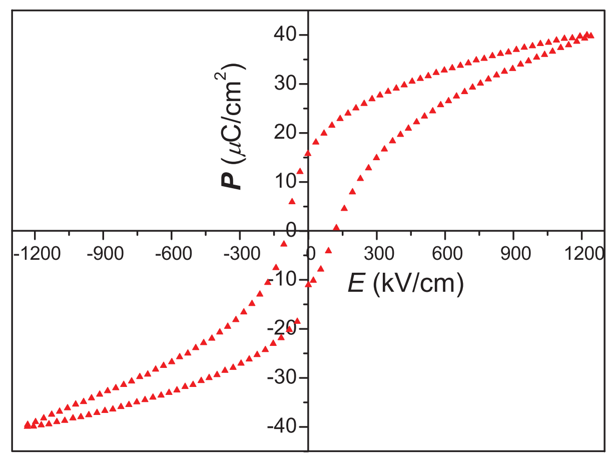

FIG. 3. Ferroelectric hysteresis loops of PZT thin film.

where A^{**}, T, q, ϕ_B, K_B, ε_0, ε_r, and E are the effective Richardson constant, absolute temperature, the electron charge, Schottky potential barrier, the Boltzmann constant, the permittivity of free space, dielectric constant (relative permittivity), and the electrical field, respectively.

Pb has a high partial pressure and can readily evaporate from lattice sites during thermal processes, leaving vacancies behind. Lead vacancies act as acceptor impurities and are considered to be one of the main sources for the leakage current in PZT thin films.[21] The defect reaction can be written as

$$Pb_{Pb} \leftrightarrow Pb + V_{Pb}^{-2} + 2h^{+}, \tag{3}$$

where Pb_{Pb} and $V_{\mathrm{Pb}}{}^{-2}$ are the lead atom in the lattice and the lead vacancy, respectively. When the injected free-carrier density exceeds the volume-generated free-carrier density (over 100 kV/cm), the main conduction mechanism is Schottky conduction associated with the free carriers trapped by the lead vacancies. The leakage current density was observed to increase rapidly above 100 kV/cm. At this electric field magnitude, sufficient injected carriers fill almost all traps generated by lead vacancies and further injected carriers exist as free carriers contributing to the leakage current.

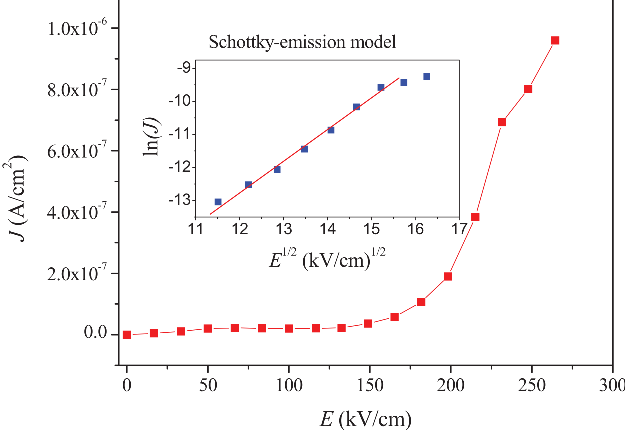

FIG. 4. J–E characteristic of PZT thin film. Inset shows the data plotted based on Schottky-emission model that produces a linear ln$J$–E$^{1/2}$ curve.

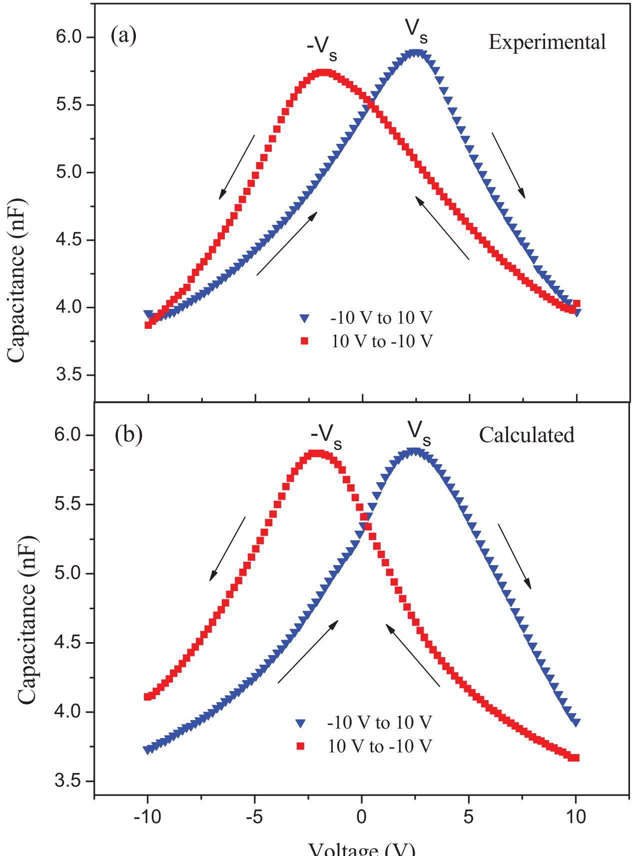

FIG. 5. C–V curve of experimental (a) and calculated (b) PZT thin film from −10V to 10 V.

Figure 5(a) shows the C–V curve of the PZT thin film at 10 kHz. When voltage is applied from −10 V to 10 V, and then from 10 V to −10 V, a butterfly-like ferroelectric capacitance variation is observed. Two polarization peaks occur that correspond to the ferroelectric measurements. $+V_s$ and $-V_s$ are the positive and negative switching biases corresponding to the coercive field and associated with polarization switching. These voltages describe the transition of reverse junction capacitance between top and bottom electrode with the Schottky model. The capacitance of this MFM system at $+V_s$ and $-V_s$ is slightly asymmetric. This may be the result of Pb vacancies (acceptor impurities). When voltage is applied from −10 V to 10 V, injected carriers will fill the traps generated by lead vacancies, decreasing the acceptor doping density. Consequently, when voltage is applied from 10 V to −10 V, the accumulation of effective charge will decrease accordingly, leading to a slight drop of the capacitance at $-V_s$.

A modified C–V model was developed for the poled ferroelectric with voltage applied in the polarization direction based on the MFM system with Schottky contacts. Fig. 6(a) shows a schematic drawing of the MFM system, Fig. 6(b) the equivalent circuit typically used, and Fig. 6(c) a proposed capacitance model for the PZT capacitor. For the model of the MFM structure of PZT film, the equivalent-circuit includes a capacitance in parallel with a resistance. When the leakage current is very low, the resistance approaches infinity. Consequently, the resistance produces a negligible effect on the C–V model at low voltage.

20 January 2026 12:52:18

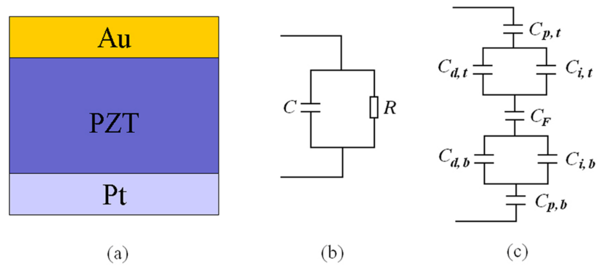

FIG. 6. Electrical characterization model of PZT thin film. (a) Schematic drawing of MFM structure, (b) regular equivalent circuit of MFM system, (c) static capacitance model including the depletion charge (C_d), polarization charge (C_p), interface-trap charge (C_{it}), and electrical domain (C_F) capacitances. The indices t and b refer to top and bottom electrodes.

The standard equivalent circuit (Fig. 6(b)) does not model the individual effects of the metal contacting the PZT. The PZT has semiconducting characteristics. In this case, a built-in electric field (E_{bi}) will form at the metal-semiconductor contacts creating a depletion layer. In the top and bottom of the system, the directions of E_{bi} are opposite (from metal to PZT film in both cases). Based on this model, a static capacitor model was established as shown in Fig. 6(c). The model includes the depletion charge (C_d), polarization charge (C_p), interface-trap charge (C_{it}), and electrical domain (C_F) capacitances. The electric domain contribution to dielectric permittivity has been described previously, but to our knowledge, it has not been included in a capacitance model of thin films.

The electric domain capacitance (C_F) is associated with domain walls within the PZT thin film. When a bias is applied, dipoles in the PZT thin film will reorient. Large-scale reorientation through domain wall motion requires less energy than homogeneous reorientation of the dipoles. Although the material is driven toward a single domain state by a high electric field, the single domain state is difficult or impossible to achieve in a ferroelectric polycrystalline system.[23,24] There is a characteristic width associated with domain walls that arises from the increased energy associated with polarization gradients balancing the crystal structure energy, and when the film thickness is smaller than this, width domains formation is constrained. There is also a surface effect on polarization associated a depletion zone. Charge accumulating within domain walls and a change of the dielectric permittivity associated with the highly distorted unit cells of the domain walls contribute to the total capacitance in thicker films. In Ref. 11, Tayebi *et al.* established a *C–V* model for ultra thin PZT film (17 nm) without an electrical domain capacitance (C_F). The domain capacitance was not needed, because domains in ultra thin PZT film are unstable and can be easily affected by an antiparallel built-in electric field[11] because the depletion layer width is comparable with the remaining thickness of the ultra thin film. This makes the effective electrical domain capacitance difficult to form, and thus, the electrical domain capacitance can be neglected in the ultra thin film. On the contrary, in the *C–V* model for our 750 nm film, the built-in electric field has less influence on the domains because the depletion layer width is much smaller than that of the remaining part of the film. As a consequence, the electrical domain capacitance (C_F) needs to be taken into consideration in our PZT thin film. This suggests that there is a critical thickness above which C_F must be included.

In the Schottky metal−semiconductor contacts, the depletion layer width (W) and depletion layer capacitance (C_d) from an AC signal are defined as[12,22]

$$W = \sqrt{\frac{2\varepsilon_0\varepsilon_r}{qN_a}(V_{bi}+V_A)}, \tag{4}$$

$$C_d = \frac{\varepsilon_0\varepsilon_r A}{W} = \frac{\varepsilon_0\varepsilon_r A}{\sqrt{\frac{2\varepsilon_0\varepsilon_r}{qN_a}(V_{bi}+V_A)}}, \tag{5}$$

where ε_0, ε_r, A, N_a, V_{bi}, V_A, and q are the permittivity of free space, the dielectric constant of the PZT film, the electrode area, the equivalent acceptor doping density, the built-in potential of the Schottky barrier, the applied bias, and the charge, respectively. The built-in potential can be expressed as follows:[11,22]

$$V_{bi} = \frac{\chi_{PZT}}{q} + \left(\frac{E_{C(PZT)} - E_{F(PZT)}}{q}\right) - \frac{\phi_M}{q}, \tag{6}$$

where χ_{PZT}, $E_{C(PZT)}$, and $E_{F(PZT)}$ are the affinity, conduction band, and Fermi energies of the PZT film, and ϕ_M is work function of the metal top/bottom electrode.

The interface polarization capacitance (C_p) resulting from polarization charges within an ultrathin layer from the metal electrode, referred to as the dead layer δ, is given by[11]

$$C_P = \frac{\varepsilon_0\varepsilon_r A}{\delta}. \tag{7}$$

Interfacial trap capacitance (C_{it}) originating from interface defects coexists in parallel with C_p.

According to Gauss theory, electric domain capacitance (C_F), originating from the charge accumulation and modified polarization reorientation within domain walls, can be described by[25]

$$C_F = \frac{dQ}{dV} = A\left(\frac{\varepsilon_0\varepsilon_r}{t_F} + \frac{dP}{dV}\right), \tag{8}$$

where t_F is effective width of electric domain capacitance, which is equal to the total thickness of PZT thin film minus the depletion layer width.

As the bias is varied, the total capacitance will be composed of reverse and forward biased junction capacitances corresponding to up and down polarizations, respectively. When the bottom electrode is grounded and −10 V is applied to the top electrode, the external electric field (E_a) is from bottom to top, which will decrease the thickness of the top depletion layer and expand that of the bottom depletion layer. When applying +10 V voltage to the top electrode, the situation will change to the opposite. So, when applying voltage from –10V to +10 V in the *C–V* curve, the capacitor model of the system is dominated by the model shown in Fig. 7. With the increasing of applied voltage, the capacitor

20 January 2026 12:52:18

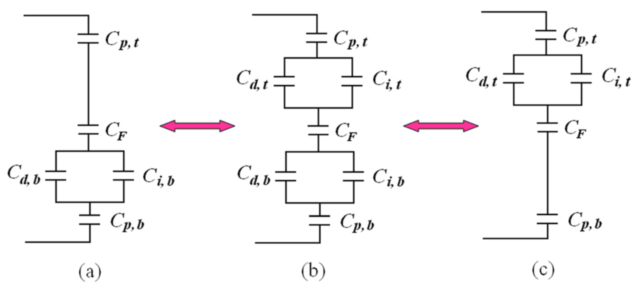

FIG. 7. Dynamic capacitance model of PZT thin film at various bias. (a) −10 V, (b) ∼0 V, and (c) 10 V.

model will evolve as depicted as shown in the model Figs. 7(a)–7(c) dynamically.

Parameters were determined for the *C–V* model of the PZT thin film and a simulation was performed. C_d and C_p were calculated using Eqs. (4)–(7). C_{it} originating from interface traps can coexist in parallel with C_d if reactive (oxidizing) metals such as Ti are used as electrodes,[11] so here, C_{it} was neglected relative to C_d. The *P–V* curves (down and up) of PZT thin film from both −10 V to 10 V and 10 V to −10 V were fit to determine the differential (d*P*/d*V*) and obtain C_F using Eq. (8). The frequency of the *C–V* model parameters are in accordance with that of *P–V* measurement of 1 kHz, and no attempt was made to extend the model to other frequencies. The resulting parameters are $\varepsilon_r = 428$, $A = 1 \times 10^{-6}$ m^2 (the area of Au electrode), $\delta = 12.1$ nm, $N_a = 0.34 \times 10^{20}$/cm^3, $\chi_{PZT} = 3.5$ eV, $\phi_{M(Pt)} = 5.3$ eV (bottom electrode), and $\phi_{M(Au)} = 5.1$ eV (top electrode), $E_{C(PZT)} - E_{F(PZT)} = 2.0$ eV.[11,12,26] The results are shown in Fig. 5(b), which is similar to the experimental curve (Fig. 5(a)), indicating that the capacitor network model represents the dominant contributions to the *C–V* behavior of ferroelectrics with bistable polarization states.

IV. CONCLUSION

In summary, dense, homogeneous, and crack-free ferroelectric PZT thin film with ⟨*h*00⟩-preferred orientation were obtained by using the sol-gel method. The volume fraction $\alpha_{(100)}$ of (*h*00) oriented grains in PZT film was approximated [$\alpha_{(100)} \approx 80\%$] from XRD results of PZT thin film and powder. The PZT thin film exhibited good ferroelectric *P–E* loops. With a cyclic voltage of 95 V, the $2P_r$ and $2E_c$ of PZT thin film were 28 μC/cm^2 and 240 kV/cm, respectively. The PZT thin film showed a low leakage current density from 10^{-8} A/cm^2 to 10^{-7} A/cm^2. The conductive behavior was dominated by Schottky-emission with deep traps from 100 kV/cm to 250 kV/cm. A dynamic capacitance model, in which an electrical domain capacitance (C_F) was taken into consideration, was established based on a MFM system with Schottky-contacts. The introduction of domain capacitance (C_F) into the model is required for thicker films and not for ultra thin films. This suggests there is a critical thickness in ferroelectric film above which C_F must be included. Parameters were experimentally determined for the capacitance model and it was shown to reproduce the observed *C–V* behavior.

ACKNOWLEDGMENTS

This work was supported by NSF Nanosystems Engineering Research Center for Translational Applications of Nanoscale Multiferroic Systems (TANMS) Cooperative Agreement Award No. EEC-1160504.

[1]J. F. Scott, Science **315**, 954 (2007).
[2]P. Maksymovych, S. Jesse, P. Yu, R. Ramesh, A. P. Baddorf, and S. V. Kalinin, Science **324**, 1421 (2009).
[3]E. Y. Tsymbal and A. Gruverman, Nat. Mater. **12**, 602 (2013).
[4]M. Dawber, K. M. Rabe, and J. F. Scott, Rev. Mod. Phys. **77**, 1083 (2005).
[5]M. D. Nguyena, M. Dekkersb, H. N. Vua, and G. Rijndersb, Sens. Actuators A **199**, 98 (2013).
[6]Y. Bastani and N. Bassiri-Gharb, Acta Mater. **60**, 1346 (2012).
[7]L. Feigl, E. Pippel, L. Pintilie, M. Alexe, and D. Hesse, J. Appl. Phys. **105**, 126103 (2009).
[8]L. H. Xu, D. D. Jiang, and X. J. Zheng, J. Appl. Phys. **112**, 043521 (2012).
[9]A. Bose, M. Sreemany, and S. Bysakh, Appl. Surf. Sci. **282**, 202 (2013).
[10]J.-R. Cheng, W. Zhu, N. Li, and L. E. Cross, Appl. Phys. Lett. **81**, 4805 (2002).
[11]N. Tayebi, S. Kim, R. J. Chen, Q. Tran, N. Franklin, Y. Nishi, Q. Ma, and V. Rao, Nano Lett. **12**, 5455 (2012).
[12]L. Pintilie, I. Boerasu, M. J. M. Gomes, T. Zhao, R. Ramesh, and M. Alexe, J. Appl. Phys. **98**, 124104 (2005).
[13]S. Sun and T. S. Kalkur, IEEE Trans. Ultrason. Ferroelectr. **51**, 786 (2004).
[14]C. D. E. Lakeman and D. A. Payne, J. Am. Ceram. Soc. **75**, 3091 (1992).
[15]R. A. Wolf and S. Trolier-McKinstry, J. Appl. Phys. **95**, 1397 (2004).
[16]K. G. Brooks, I. M. Reaney, R. Klissurska, Y. Huang, L. Bursill, and N. Setter, J. Mater. Res. **9**, 2540 (1994).
[17]C. J. Lu, Y. Qiao, Y. J. Qi, X. Q. Chen, and J. S. Zhu, Appl. Phys. Lett. **87**, 222901 (2005).
[18]Y. Bastani, T. Schmitz-Kempen, A. Roelofs, and N. Bassiri-Gharb, J. Appl. Phys. **109**, 014115 (2011).
[19]M. D. Nguyen, H. Nazeer, M. Dekkers, D. H. A. Blank, and G. Rijnders, Smart Mater. Struct. **22**, 085013 (2013).
[20]S. M. Sze and K. K. Ng, *Physics of Semiconductor Devices*, 3rd ed. (John Wiley &Sons, Hoboken, NJ, 2006).
[21]Z. Zhang, P. Wu, L. Lu, and C. Shu, Appl. Phys. Lett. **88**, 142902 (2006).
[22]R. S. Muller and T. I. Kamins, *Device Electronics for Integrated Circuits*, 3rd ed. (John Wiley & Sons, Hoboken, NJ, 2007).
[23]F. X. Li and R. K. N. D. Rajapakse, J. Appl. Phys. **101**, 054110 (2007).
[24]J. L. Jonesa, M. Hoffman, and K. J. Bowman, J. Appl. Phys. **98**, 024115 (2005).
[25]C. Zheng and T. Ting-Ao, Ferroelectrics **197**, 111 (1997).
[26]N. G. Apostol, L. E. Stoflea, G. A. Lungu, L. C. Tanase, C. Chirila, L. Frunza, L. Pintilie, and C. M. Teodorescu, Thin Solid Films **545**, 13 (2013).

20 January 2026 12:52:18